PIER C

(Received 30 August 2025, Accepted 11 November 2025, Scheduled 8 December 2025)

Optimized Multi-Layers Inversion Scheme for Azimuthal Resistivity Logging-While-Drilling Based on Supervised Descent Method

Yongsheng Xu[1], Yuehui Li[1,*], Junyuan Zheng[1], Xiangyang Sun[2], Peng Hao[2], and Jie Ren[1]

[1]*School of Computer and Software Engineering, Xihua University, Chengdu 610039, China*
[2]*School of Electronic Science and Engineering, University of Electronic Science and Technology of China, Chengdu 611731, China*

ABSTRACT: Logging-While-Drilling (LWD) azimuthal resistivity measurements deliver critical support for geosteering in complex hydrocarbon reservoirs by acquiring real-time azimuthal responses of formation electrical properties around the borehole; the precision and efficiency of its inversion directly govern the reliability of horizontal well trajectory optimization strategies. Currently, the inversion study of azimuthal resistivity logging with drilling mainly focuses on the simplified three-layer stratigraphic model, and this simple layered model and limited stratigraphic parameter settings have been difficult to adapt to the needs of the increasingly complex geological exploitation. However, inversion of complex multilayer formations ($\geq$ 5 strata) confronts three main challenges: high-dimensional parameterization, attenuated response sensitivity, and noise-impaired accuracy. These constraints compromise field-applicable accuracy thresholds for multilayer stratigraphic inversion. To address the above problems, in this paper, by combining the advantages of traditional inversion methods with machine learning concepts, a new optimized supervised descent inversion method is proposed for azimuthal resistivity LWD in a five-layer formation model. The data-adaptive reconstruction algorithm enhances outer formation response sensitivity. The subsequent integration of multi-matrix fusion with secondary inversion optimization further augments accuracy in field well-log inversion. Numerical simulations and downhole measurements verify the effectiveness of the proposed method, which is a field-deployable real-time inversion algorithm with higher accuracy and stronger noise immunity.

1. INTRODUCTION

Geosteering leveraging azimuthal resistivity LWD delivers critical decision support for real-time trajectory optimization of horizontal wells through the instantaneous interpretation of near-borehole formation properties. This technology now constitutes the cornerstone for the efficient development of complex hydrocarbon reservoirs [1, 2]. Functioning as an "information decoder" (formation parameter extractor) for geosteering, the precision and computational efficiency of azimuthal electromagnetic LWD data inversion directly dictate the reliability of real-time operational decisions [3, 4]. During downhole logging operations, electromagnetic wave propagation is severely contaminated by substantial external noise. This contamination significantly degrades measured signals, drastically reducing the volume of valid inversion-response data while amplifying noise interference. Consequently, inversion accuracy undergoes substantial deterioration. Existing methods cannot achieve satisfactory inversion results for five-layer formations in actual wells. Traditional inversion methods exhibit significant limitations: deterministic algorithms such as the Gauss-Newton (GN) method [5], despite possessing rigorous mathematical foundations, require frequent forward modeling during iterations. This results in single-step inversion durations of several minutes, failing to meet the second-level response requirements of actual drilling operations [6–8]. Although data-driven deep learning algorithms (e.g., CNN, ResNet, PNN) enable millisecond-level prediction via offline training, their "black-box" nature results in inadequate noise resistance, leading to non-physical interpretations in complex downhole electromagnetic environments involving vibration and mud invasion [9–11]. These issues are particularly pronounced in the inversion of deep complex stratigraphic structures (e.g., multi-angle faults and thin interbeds), thus urgently necessitating the development of novel inversion methods that integrate high precision, robustness, and physical consistency.

The emergence of the supervised descent method offers a novel solution [12]. By integrating traditional deterministic inversion approaches with machine learning characteristics, this method demonstrates significant advantages in addressing multilayer formation inversion challenges. Initially proposed in [13], the supervised descent method was subsequently optimized by Hu et al. and Guo et al. for directional electromagnetic logging applications [14, 15]. Compared to the traditional gradient descent method [16] — which is prone to converging to local optima — and machine learning's vulnerability to overfitting due to heavy reliance on simulated data, this approach initially learns and records the descent direction of the objective function within the training set. It subsequently leverages this direction to directly update the target model for solving optimization problems.

* Corresponding author: Yuehui Li (liyuehui@xhu.edu.cn).

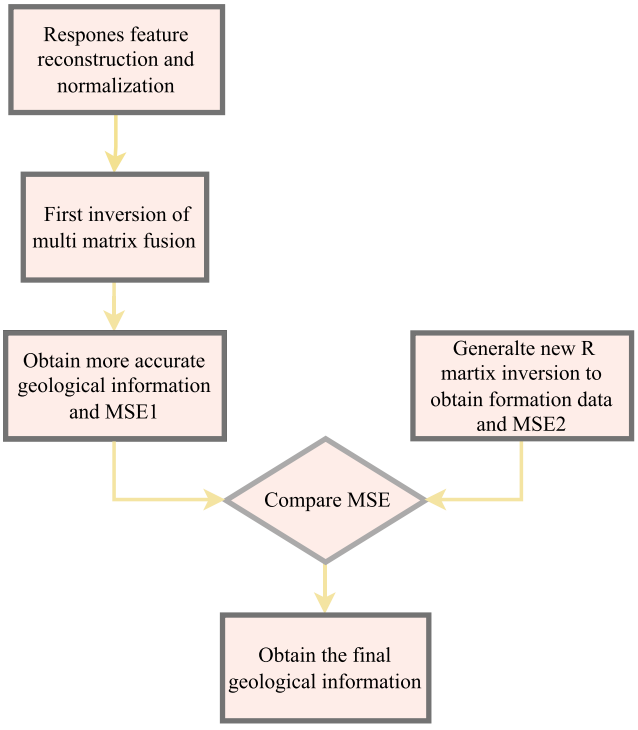

FIGURE 1. Method flowchart.

However, existing supervised descent methods are predominantly confined to three-layer formation models, whereas deep exploration in practical logging operations demands overcoming the high-precision inversion bottleneck for formations of five or more layers. Five-layer formation inversion currently faces three major challenges: (1) The inversion parameters have expanded from five dimensions (two boundary depths + three resistivities) to nine dimensions (four boundary depths + five resistivities) while the number of measurement responses remains unchanged. This dimensional mismatch leads to an ill-posed inversion condition, which often results in non-unique solutions. (2) Outer formation layers exhibit low signal sensitivity. Conventional supervised descent methods demonstrate insufficient accuracy when inverting the outermost resistivity boundaries. (3) Increased parameter dimensionality exponentially amplifies noise interference, frequently generating outlier solutions that degrade inversion precision. To address these challenges, this paper proposes an enhanced Supervised Descent Inversion method with dual innovations: Multivariate Signal Recomposition for data augmentation, preprocessing response signals expands the measurement dataset, effectively resolving the dimensionality mismatch (insufficient responses vs. excessive unknowns) that causes pathological inversion. Moreover, this approach enhances the sensitivity of measurement signals to outermost resistivity boundaries, ensuring significantly improved accuracy for inverting these critical parameters. Second, the algorithm employs multiple optimization strategies: it first performs an initial inversion to validate formation data, then selects statistically screened data subsets to train the matrix and conduct a secondary inversion. Ultimately, it chooses the optimal result from both inversion outcomes through error comparison, thereby reducing accuracy degradation caused by noise interference.

The subsequent sections of this paper are structured as follows. After analyzing traditional supervised descent inversion methods, we detail the design process of our proposed approach. Next, we validate the method's effectiveness through simulation cases and real-well data. Finally, we summarize the research findings.

2. THEORY AND METHODS

This section begins by introducing the modeling framework of the logging instrument employed. Building upon an overview of the traditional supervised descent method, we elaborate on the specific procedures of the optimized supervised descent approach proposed in this study. We initially preprocess the dataset by reconstructing response characteristics, subsequently execute the first inversion via multi-matrix fusion, and ultimately derive accurate inversion results through secondary inversion. The detailed workflow is illustrated in Fig. 1.

2.1. Instrument Model

The azimuthal logging-while-drilling system employs a multi-frequency, multi-spacing coil array configuration [17, 18]. As depicted in Fig. 2, the tool integrates four transmitter coils ($T1, T2, T3, T4$) and four receiver coils ($R1, R2, R3, R4$). With five axial transmitter-receiver spacing configurations (0.5–2.4 m) operating at 100 kHz, 400 kHz, and 2 MHz frequencies through time-division multiplexing, the system acquires multiple response signals. Due to downhole real-time transmission constraints, eight characteristic curves are generated: four apparent resistivity curves and four geosteering signal curves. The apparent resistivity curves dynamically characterize circumferential formation resistivity distribution by reflecting electromagnetic responses at varying depths of investigation, while the geosteering signals precisely locate the tool relative to lateral formation boundaries. As depicted in Fig. 3, the aforementioned eight responses enable the inversion of resistivity for two outer layers, two inner layers, and one intermediate layer, along with four formation boundaries ($h1$–$h4$). For forward modeling of this tool, responses are rapidly computed using Green's function-based methods for planar layered media. These solutions will serve as training datasets for parameter inversion during subsequent data interpretation.

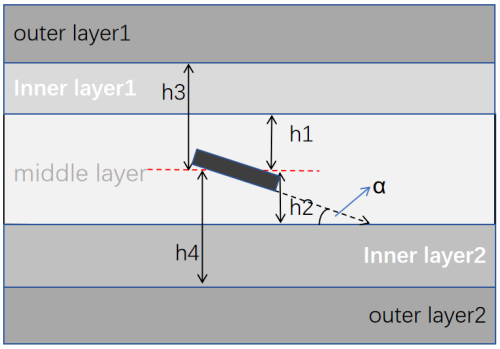

FIGURE 2. Structure model of instrument.

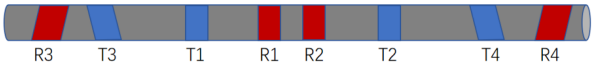

FIGURE 3. Stratigraphic model diagram.

2.2. SDM Inversion

For electrical logging data inversion, the currently employed Supervised Descent Method (SDM) represents a hybrid algorithm integrating physics-driven inversion with data-driven machine learning. This approach significantly enhances the efficiency and stability of complex formation parameter inversion. Compared to deterministic inversion methods such as Newton's method, SDM incorporates prior knowledge into global descent gradients via offline training. This eliminates computationally intensive Hessian and Jacobian matrix calculations required in Newtonian solvers, enabling rapid global convergence for arbitrary initial estimates. In contrast to purely machine learning-based methods such as artificial neural networks [19, 20], SDM substantially reduces the demand for training data while effectively mitigating the risk of overfitting attributable to the black-box nature of neural networks.

In Logging While Drilling inversion, the objective function $C(x)$ is conventionally defined as:

$$C\left(x\right)=\frac{1}{2}\left\|F\left(x\right)-m\right\|^{2} \tag{1}$$

Let x denote the formation parameters to be inverted, while m represents the vector of observed logging measurements (e.g., resistivity, acoustic transit time). The physical forward model $F(x)$ mathematically maps formation parameters to observational responses. Performing a second-order Taylor expansion of the objective function and minimizing it by setting the gradient to zero yields:

$$\begin{aligned}\Delta x&=-H_C(x)^{-1}J_C(x)\\ -H_C(x)^{-1}J_C(x)&=-2H_C(x)^{-1}J_S(x)^T(F(x)-m)\end{aligned} \tag{2}$$

where $H_C(x)$ is the Hessian matrices of $C(x)$, and $J_S(x)$ is the Jacobian matrix of $F(\cdot)$. Therefore, using a predefined sample dataset $\{x_{\text{train}}, F(x_{\text{train}})\}$, SDM iteratively learns statistical descent directions and generates: $R=-2H_C(x)^{-1}J_S(x)^T$ where x_{train} denotes model parameters, and $F(x_{\text{train}})$ represents corresponding forward responses. Therefore, in the kth iteration of the training procedure, the update step can be represented as:

$$\Delta x_k=R_k\left(F(x_k)-m\right) \tag{3}$$

The average descent direction R of N training samples can be obtained by minimizing:

$$\arg\min_{R_k}\left(\sum_{n=1}^{N}\left\|x_k^n-R_k\Delta m_k^n\right\|^2\right) \tag{4}$$

where $\Delta x_k^n=x_{\text{train}}^n-x_k^n$, $\Delta m_k^n=F(x_k^n)-F(x_{\text{train}}^n)$ in which x_k^n is the nth updated parameters in the kth iteration, and $F(x_k^n)$ is the corresponding forward responses of x_k^n. Solving this linear least squares problem, we can obtain:

$$R_k=\left(\Delta M_k^T\Delta M_k\right)^{-1}\Delta M_k^T\Delta x_k \tag{5}$$

where $\Delta x_k=\left[\Delta x_k^1,\Delta x_k^2,\Delta x_k^3...\Delta x_k^n\right]$, $\Delta M_k=\left[\Delta M_k^1,\Delta M_k^2,\Delta M_k^3...\Delta M_k^n\right]$. Thus, by preserving the statistical average descent direction during each iteration, the offline training phase for formation parameter inversion is completed.

2.3. Regularization

When applying the Supervised Descent Method (SDM) to actual well data, significant challenges arise — particularly the ill-posed nature of inversion interpretation [21]. This ill-posedness frequently causes instability in inversion results and poor convergence behavior, severely compromising the accuracy and reliability of the inversion process. To effectively address this issue, this paper proposes a dynamic regularization scheme to improve the accuracy of supervised descent results. Specifically, this involves modifying the optimization problem in Equation (4) and introducing a regularization parameter λ_k [22].

$$\arg\min_{R_k}\left(\sum_{n=1}^{N}\left\|x_k^n-R_k\Delta m_k^n\right\|^2\right)+\lambda_k\left\|R_k\right\|^2 \tag{6}$$

The primary role of these parameters is to dynamically recalibrate term weights within the objective function, thereby refining the inversion process through balanced term interactions. To implement this mechanism, our dynamic regularization scheme autonomously evolves with successive iterations, with its update rule defined as:

$$\lambda_k=\lambda_0 q^k,\quad 0<q<1 \tag{7}$$

Within this formulation, λ_k denotes the initial regularization parameter governing baseline constraint intensity, while q characterizes the exponential decay rate governing progressive relaxation during iterative refinement.

2.4. Response Characteristics Reconstruction

The five-layer formation inversion faces compounded challenges including heightened model complexity, proliferation of inversion parameters, and increased stratigraphic layering. These induce: (1) escalated computational demands from expanded parameter dimensionality, (2) amplified solution uncertainty due to sparse logging responses, and (3) progressive attenuation of outer-layer parameter sensitivity degrading inversion accuracy. To overcome these constraints, this study initially normalizes input data to mitigate nonlinear effects in response signals. Subsequently, it reconstructs logging responses using mathematical metrics (variance, maxima, peak-to-trough amplitudes), thereby expanding the dataset. Through sensitivity analysis, characteristic responses demonstrating heightened sensitivity to formation boundaries and resistivity are identified [23]. After feature reconstruction, the number of response data has increased from the original m to the current $m+n$

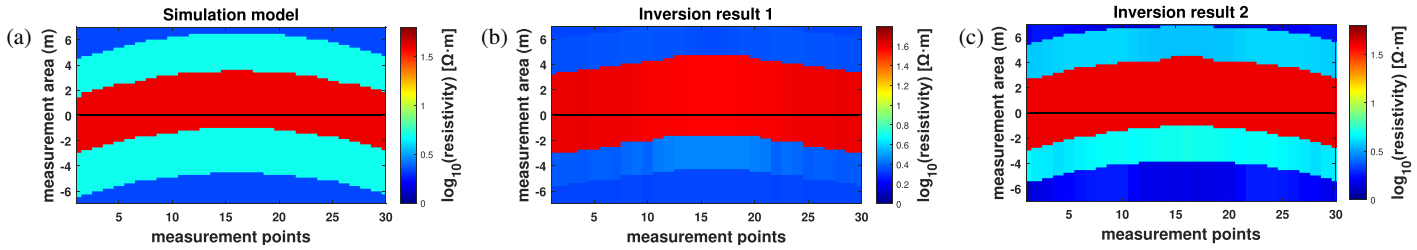

FIGURE 4. The graphical representation of reservoir inversion with changed response characteristics.

(m represents the number of initial measured responses, and n represents the number of newly generated responses). This increases the dimension of the training matrix R, providing high-precision inversion for complex real-time geosteering.

2.5. Multi-Matrix Fusion Scheme

The multi-matrix fusion scheme enhances inversion fidelity by addressing the limitation in traditional supervised descent methods where a single matrix cannot simultaneously achieve wide resistivity coverage and high-precision inversion. In edge detection inversion, instruments typically operate within formations featuring high-resistivity middle layers sandwiched between low-resistivity strata. During training, the high-resistivity zone ($> 10\,\Omega$·m) of matrix R is decomposed into n contiguous subdomains ($\Omega = \sum \Omega_K$), with dedicated inversion matrices independently trained per subdomain to substantially reduce training errors in high-resistance regions, while the low-resistivity range (1–10 Ω·m) remains undecomposed due to gradual response variations, preventing excessive matrix proliferation. During online inversion, the apparent resistivity curve within the response profile enables effective determination of the instrument's current formation resistivity range, facilitating targeted R matrix selection. This process ultimately yields formation resistivity measurements with enhanced precision.

2.6. Secondary Inversion Scheme

Although the multi-matrix fusion scheme demonstrates significant accuracy improvements for resistivity characterization, its enhancement of boundary definition remains suboptimal. The integration of secondary inversion enhances wellbore inversion precision through the following procedure: During actual well logging, formation parameters undergo initial rapid inversion via neural networks or supervised descent methods, generating resistivities $\Omega_1, \Omega_2, \Omega_3 ... \Omega_5$ and formation boundaries L_1, L_2, L_3, L_4. These parameters then drive boundary redefinition to retrain the gradient matrix, establishing constrained ranges, and let $\Omega_{\text{down}} < \Omega_i < \Omega_{\text{up}}$, $L_{\text{down}} < L_i < L_{\text{up}}$ (where Ω_{down} and Ω_{up} denote redefined lower/upper resistivity boundaries, L_{down} and L_{up} corresponding formation boundary limits). Subsequently, randomized samples are regenerated within this narrowed parameter space. Sample range selection proves particularly critical in this context. Given the inherent imprecision of initial inversion results, an excessively narrow range may lead to substantial deviation during secondary inversion, as the retraining dataset for the resistivity matrix could significantly depart from ground truth values. Conversely, an overly broad range yields negligible refinement in the secondary inversion outcomes. Consequently, to enhance inversion accuracy, it is imperative to both improve the reliability of the initial inversion and ensure appropriate sample range selection. For heightened initial result fidelity, we employ the multi-matrix fusion SDM method (Section 2.5), which significantly refines the precision of resistivity and boundary characterization obtained from the primary inversion. To ensure appropriate sample range selection, we implement proportional scaling to constrain resistivity and boundary parameters within x to y times of their original ranges. Here, x and y denote expansion factors for resistivity Ω_i and formation thickness L_i, respectively. The scaling constraints are defined as: $x * \Omega_i < \Omega_i < y * \Omega_i$; $x * L_i < L_i < y * L_i$ where x and y denote the lower-bound and upper-bound scaling factors, respectively. In field exploration, significant noise contamination during signal propagation through formations — or inherent measurement errors in acquired responses — often introduces deviations in the initial inversion results. These noisy reconstructions may propagate systematic errors, consequently compromising the fidelity of subsequent inversion stages. To prevent error accumulation, we introduce the Mean Square Error (MSE) parameter defined as the L2-norm of the difference between field-acquired response S_{measure} and synthetic response $S_{\text{inversion}}$ from forward modeling of simulated formations.

$$\text{MSE} = \|S_{\text{measure}} - S_{\text{inversion}}\|^2 \tag{8}$$

3. NUMERICAL RESULTS AND ACTUAL WELL TEST RESULTS

Sections 3.1–3.3 exclusively employ synthetic data generated by our in-house forward modeling program, while Section 3.4 utilizes field-acquired well log data obtained through actual formation exploration.

3.1. Effect of Preprocessing on Response Data

This study employs a multi-feature signal reconstruction-based data enrichment approach. By extracting physico-mathematical attributes from raw response data — including gradients, head-to-tail differentials, anomaly features, and variance — the original eight response curves (apparent resistivity and geological signal curves) are expanded to ten curves. These enhanced curves exhibit heightened sensitivity to outer formations and resistivity, yielding significantly improved inversion accuracy compared to the original dataset.

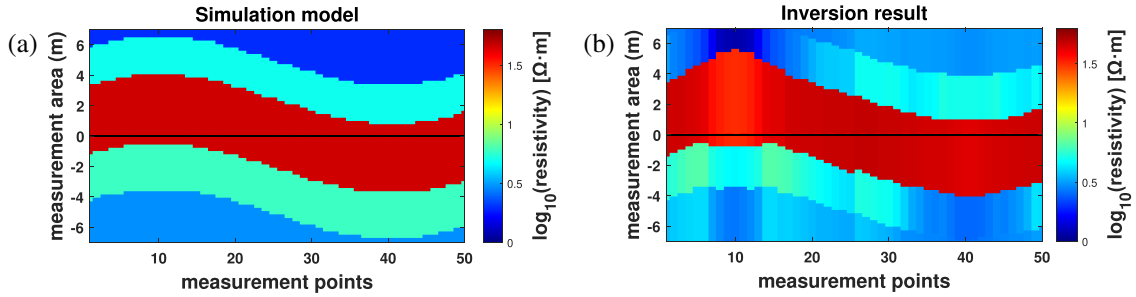

FIGURE 5. The layered inversion effect with multi-matrix fusion incorporated.

Fig. 4(a) depicts a five-layer synthetic formation model serving as the ground truth. Fig. 4(b) presents the inverted formation model derived from the original eight responses, exhibiting substantial deviations from Fig. 4(a). In contrast, Fig. 4(c) displays the inversion results utilizing the enhanced ten-response dataset obtained through preprocessing and feature expansion. Critical improvements are observed: the reconstructed formation boundaries and resistivity values in Fig. 4(c) demonstrate significantly closer correspondence to the reference model Fig. 4(a) compared to Fig. 4(b).

3.2. Experiments Incorporating Multi-Matrix Fusion into SDM Methodology

In this approach, four pre-trained matrices were employed for inversion. Given that hydrocarbon-bearing zones exhibit higher resistivity than surrounding formations in actual exploration scenarios, resistivity boundary logging is specifically designed to determine the proximity to oil/water contacts during tool traversal. Consequently, the iterative matrix R was constructed using training data featuring a central high-resistivity layer flanked by low-resistivity formations to optimize boundary detection. The four matrices are designated as $R1$, $R2$, $R3$, and $R4$, with high-resistivity training ranges configured as follows: $R1$ covers 10–20 Ω·; $R2$ spans 20–30 Ω·m; $R3$ operates within 30–40 Ω·m; and $R4$ extends across 40–60 Ω·m. The low-resistivity training range for all four matrices is uniformly set at 0–10 Ω·m. Key parameters are detailed in Table 1, with each matrix trained on 1,500 samples. Using forward modeling, we constructed a 50-point formation model Fig. 5(a) with the middle layer (red zone) fixed at 45 Ω·m, while the four flanking layers exhibit randomized resistivity values within 0–10 Ω·m. Following preprocessing with the multi-feature signal reconstruction (Section 3.1), the multi-matrix fusion inversion yields the results in Fig. 5(b). Notably, both resistivity distribution and formation boundaries demonstrate enhanced alignment with the synthetic model in Fig. 5(a). Moreover, the resistivity exhibits significantly enhanced contrast compared to that in Fig. 5(b).

TABLE 1. Training ranges of the R matrices.

R	high-resistance Ω·m	low-resistance Ω·m	boundary m
$R1$	10–20	1–10	0.5–5
$R2$	20–30	1–10	0.5–5
$R3$	30–40	1–10	0.5–5
$R4$	40–50	1–10	0.5–5

3.3. Comparative Experiments with Quadratic Inversion Optimization Algorithm

Analysis of the two aforementioned methods reveals that inversion using the R-matrix trained on resistivity datasets within selected ranges produces results with improved alignment to the synthetic model. Nevertheless, achieving satisfactory accuracy in both formation boundary delineation and resistivity quantification remains challenging. To address this limitation, we implement the quadratic inversion algorithm (Section 2.6) while simultaneously constraining both boundary and resistivity dataset ranges. Validation is performed through comparative studies on two synthetic formation models. Case 1 features a five-layer synthetic formation model with fixed resistivity in the middle layer in Fig. 6(a). After implementing the quadratic inversion algorithm, the results were visualized. Fig. 6(b) demonstrates significantly improved resistivity matching at the peripheries and enhanced boundary accuracy compared to Fig. 5(b). Both resistivity distribution and structural boundaries exhibit superior alignment with the synthetic formation model.

Case 2 employs a formation model with dynamically varying resistivity in the intermediate layer in Fig. 6(c), designed to replicate actual well conditions where formation resistivity undergoes continuous fluctuations during exploration. This configuration enables more realistic simulation of downhole inversion scenarios. The results of the traditional supervised descent method are shown in Fig. 6(d). It can be seen that the performance of the traditional method is not good enough, with significant errors in both the boundary and resistivity changes. This demonstrates that the traditional supervised descent method produces certain errors in inversion results when resistivity undergoes substantial changes. However, when we apply the optimized supervised descent method for re-inversion as shown in Fig. 6(e), noticeable improvements are achieved in both boundary delineation and resistivity characterization.

3.4. Effect on Noise

To evaluate the effectiveness of a method in actual wells, noise resistance serves as an important criterion. In this numerical simulation, a certain amount of noise (5% Gaussian white noise) was added to the generated response data. Subsequently,

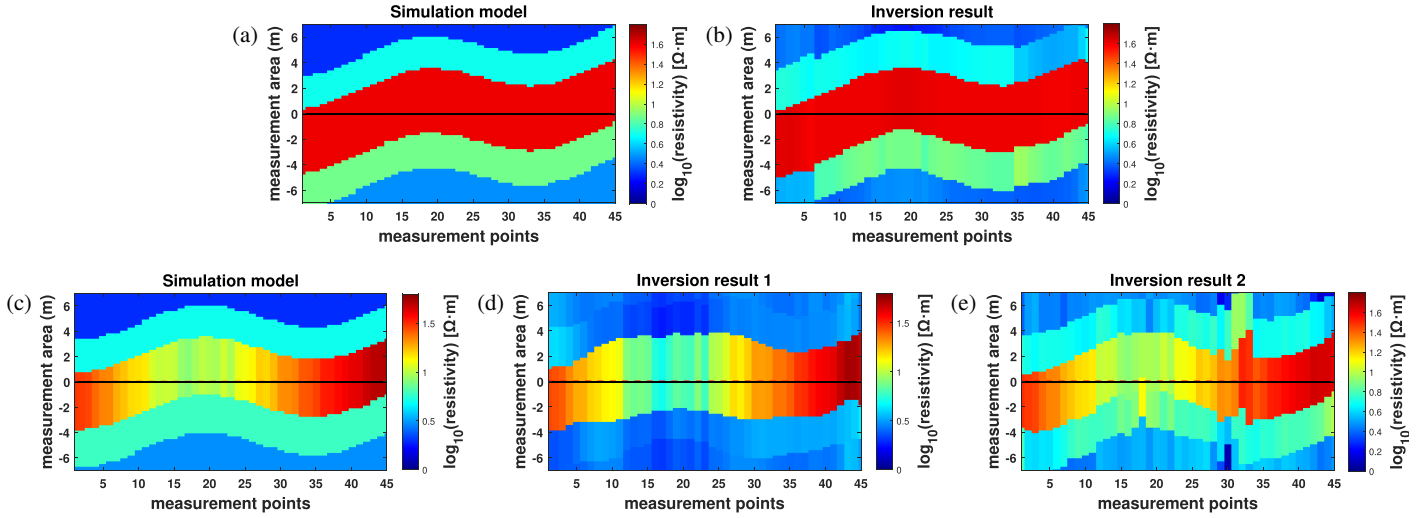

FIGURE 6. Graph of comparative experiments with secondary inversion optimization incorporated.

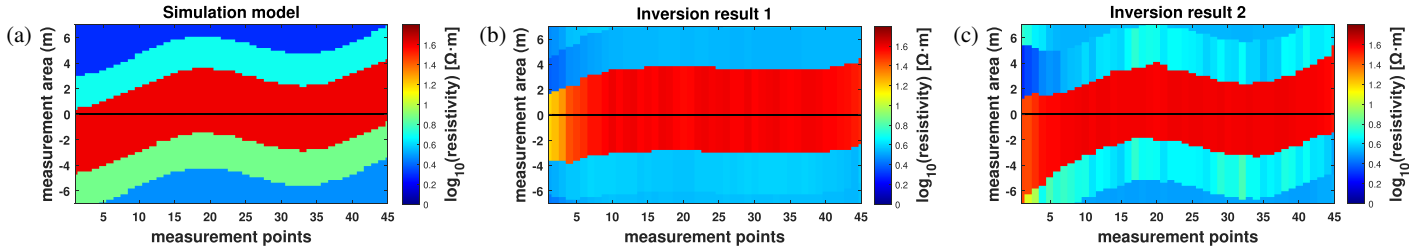

FIGURE 7. Noise inversion comparison chart.

both the conventional SDM and improved SDM methods were employed for inversion. Fig 7(a) illustrates the simulated formation model utilized in this inversion analysis. Initially, the inversion results obtained using the conventional Supervised Descent Method, as depicted in Fig 7(b), demonstrate a notable discrepancy in both resistivity and boundary inversion accuracy compared to the simulated formation model in Fig 7(a). In contrast, the inversion results of the improved supervised descent method proposed in this study (as shown in Fig 7(c)) demonstrate high precision in boundary identification and resistivity estimation, with closer alignment to the simulated formation model in Fig 7(a), indicating that the improved method maintains robust performance even under noisy conditions.

3.5. Actual Well Test Results

Most current research on electrical logging inversion techniques relies on simulation models, with few effective experimental studies conducted in real-well environments. Compared to simulation models, the greatest difficulties in real-well environments are increased noise and the heterogeneity of formations and resistivity. The following experiments will validate the effectiveness of the proposed improved SDM method based on real-well response data. Fig. 8(a) and Fig. 8(b) display response curves obtained from resistivity logging in an actual well. The logging tool transmits two sets of signals, each containing four curves, totaling eight curves. Fig. 8(a) presents four apparent resistivity signal curves (Rsl) that generally reflect variations in formation resistivity around the tool during downhole movement. Fig. 8(b) shows four geological signal curves (Gsl) indicating changes in the distance between the tool's position and formation boundaries. Using the improved supervised descent method on the aforementioned eight actual well response curves, inversion was performed with results depicted in Fig. 8(c). The apparent resistivity curves in Fig. 8(a) reveal a pattern where resistivity initially increases gradually, then plunges abruptly, and finally rises steadily. Based on the geological signal curve analysis, we observe that while advancing through the high-resistivity layer (10–20 Ω·m), the resistivity readings show a gradual increase. Subsequently, as the tool exits the high-resistivity layer and enters the low-resistivity layer, the resistivity undergoes a sharp decline. Here, a positive deflection (> 0) in the geological signal curve indicates that the formation above the tool exhibits higher resistivity while the section below exhibits lower resistivity. Finally, the tool reenters the high-resistivity layer. This phenomenon aligns with the characteristic pattern of the geological signal curve. When the curve exhibits a sustained negative deflection (overall < 0), it indicates that the formation below the tool exhibits higher resistivity while the section above shows lower resistivity. As demonstrated in Fig. 8(c) — the inversion results derived from our improvised supervised descent method — remarkable consistency is observed with both the geological signal curve Fig. 8(b) and resistivity profile. Fig. 8(a) is acquired through actual well measurements. This correlation conclu-

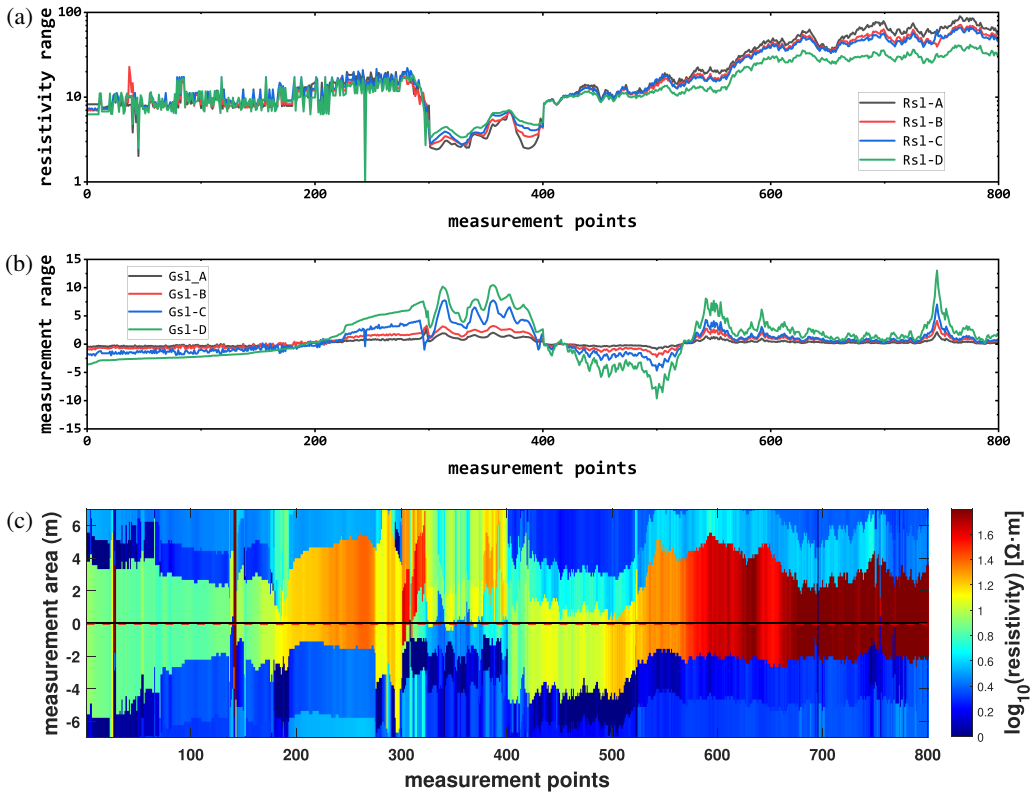

FIGURE 8. Real well inversion result chart.

sively validates the efficacy of the proposed methodology in actual well conditions.

4. SUMMARY

This paper proposes an optimized SDM achieving inversion from trilayer to multilayer formations. Actual well inversion demonstrates effective formation characterization with results conforming to logging curve patterns, significantly enhancing inversion accuracy and robustness. The optimized SDM operates in two phases: Online training: Regularization and response feature reconstruction algorithms enhance data sensitivity; Offline inversion: Multi-matrix fusion and secondary inversion algorithms iteratively refine formations. This method enables high-precision, robust inversion of complex multilayered formations in engineering applications.

ACKNOWLEDGEMENT

This work was financially supported by the National Natural Science Foundation of China (Grant No. 62371111), the Sichuan Science and Technology Program (Grant No. 2023YFH0058), the Xihua University Science and Technology Innovation Competition Project for Postgraduate Students (Grant No. YK20240151), and the Engineering Research Center for ICH Digitalization and Multi-source Information Fusion (Grant No. G3-KF2022).

REFERENCES

[1] Lesso, W. G. and S. V. Kashikar, "The principles and procedures of geosteering," in *IADC/SPE Drilling Conference*, SPE–35 051, New Orleans, Louisiana, USA, 1996.

[2] Alyaev, S., E. Suter, R. B. Bratvold, A. Hong, X. Luo, and K. Fossum, "A decision support system for multi-target geosteering," *Journal of Petroleum Science and Engineering*, Vol. 183, 106381, 2019.

[3] Lee, H. O., F. L. Teixeira, L. E. S. Martin, and M. S. Bittar, "Numerical modeling of eccentered LWD borehole sensors in dipping and fully anisotropic earth formations," *IEEE Transactions on Geoscience and Remote Sensing*, Vol. 50, No. 3, 727–735, Mar. 2012.

[4] Wang, G. L., T. Barber, P. Wu, D. Allen, and A. Abubakar, "Fast inversion of triaxial induction data in dipping crossbedded formations," *Geophysics*, Vol. 82, No. 2, D31–D45, Mar. 2017.

[5] Thiel, M. and D. Omeragic, "High-fidelity real-time imaging with electromagnetic logging-while-drilling measurements," *IEEE Transactions on Computational Imaging*, Vol. 3, No. 2, 369–378, Jun. 2017.

[6] Xing, G.-L., M.-L. Zhang, M.-F. Liu, and S.-D. Yang, "An inversion method on formation dielectric constant and resistivity by using high frequency electromagnetic wave logging," *Chinese Journal of Geophysics*, Vol. 45, No. 3, 450–460, May 2002.

[7] Thiel, M. and D. Omeragic, "2D lateral imaging inversion for directional electromagnetic logging-while-drilling measurements," *Geophysics*, Vol. 84, No. 6, D217–D230, Nov. 2019.

[8] Marquardt, D. W., "An algorithm for least-squares estimation of nonlinear parameters," *Journal of the Society for Industrial and Applied Mathematics*, Vol. 11, No. 2, 431–441, 1963.

[9] Hu, Y., J. Chen, X. Wu, and Y. Huang, "A flexible and versatile joint inversion framework using deep learning," in *SEG/AAPG International Meeting for Applied Geoscience & Energy*, Houston, Texas, USA, 2022.

[10] Zhu, G., M. Gao, F. Kong, and K. Li, "A fast inversion of induction logging data in anisotropic formation based on deep learning," *IEEE Geoscience and Remote Sensing Letters*, Vol. 17, No. 12, 2050–2054, Dec. 2020.

[11] Noh, K., D. Pardo, and C. Torres-Verdin, "Deep-learning inversion method for the interpretation of noisy logging-while-drilling resistivity measurements," *arXiv preprint arXiv:2111.07490*, 2021.

[12] Yang, H., X. Jia, I. Patras, and K.-P. Chan, "Random subspace supervised descent method for regression problems in computer vision," *IEEE Signal Processing Letters*, Vol. 22, No. 10, 1816–1820, Oct. 2015.

[13] Xiong, X. and F. De la Torre, "Supervised descent method and its applications to face alignment," in *2013 IEEE Conference on Computer Vision and Pattern Recognition*, 532–539, Portland, OR, USA, Jun. 2013.

[14] Hu, Y., R. Guo, Y. Jin, X. Wu, M. Li, A. Abubakar, and J. Chen, "A supervised descent learning technique for solving directional electromagnetic logging-while-drilling inverse problems," *IEEE Transactions on Geoscience and Remote Sensing*, Vol. 58, No. 11, 8013–8025, 2020.

[15] Guo, R., M. Li, G. Fang, F. Yang, S. Xu, and A. Abubakar, "Application of supervised descent method to transient electromagnetic data inversion," *Geophysics*, Vol. 84, No. 4, E225–E237, Jul. 2019.

[16] Levenberg, K., "A method for the solution of certain non-linear problems in least squares," *Quarterly of Applied Mathematics*, Vol. 2, No. 2, 164–168, 1944.

[17] Liu, Z., Z. Nie, X. Sun, D. Wen, and J. Tan, "A low frequency forward looking antenna array for LWD and MWD," in *2017 Progress In Electromagnetics Research Symposium — Spring (PIERS)*, 151–154, St. Petersburg, Russia, May 2017.

[18] Sun, X., Z.-P. Nie, A. Li, and X. Luo, "Analysis and correction of borehole effect on the responses of multicomponent induction logging tools," *Progress In Electromagnetics Research*, Vol. 85, 211–226, 2008.

[19] Noh, K., D. Pardo, and C. Torres-Verdín, "2.5-D deep learning inversion of LWD and deep-sensing EM measurements across formations with dipping faults," *IEEE Geoscience and Remote Sensing Letters*, Vol. 19, 1–5, 2022.

[20] Jin, Y., Q. Shen, X. Wu, J. Chen, and Y. Huang, "A physics-driven deep-learning network for solving nonlinear inverse problems," *Petrophysics*, Vol. 61, No. 01, 86–98, Feb. 2020.

[21] Tikhonov, A. N. and V. Y. Arsenin, *Solutions of Ill-posed Problems*, Winston, Washington, DC, USA, 1977.

[22] Hao, P., X. Sun, Z. Nie, X. Yue, and Y. Zhao, "A robust inversion of induction logging responses in anisotropic formation based on supervised descent method," *IEEE Geoscience and Remote Sensing Letters*, Vol. 19, 1–5, 2021.

[23] Li, J., J. Tang, and H. Liu, "Reconstruction-based unsupervised feature selection: An embedded approach," in *Proceedings of the Twenty-Sixth International Joint Conference on Artificial Intelligence*, 2159–2165, Melbourne, Australia, Aug. 2017.